

High-pressure Phase Stability and Superconductivity of Pnictogen Hydrides and Chemical Trends for Compressed Hydrides

Yuhao Fu,^{1,*} Xiangpo Du,^{2,*} Lijun Zhang,^{1,2,†} Feng Peng,² Miao Zhang,² Chris J. Pickard,³ Richard J. Needs,⁴ David J. Singh,^{1,5,‡} Weitao Zheng,¹ and Yanming Ma^{2,§}

¹*College of Materials Science and Engineering and Key Laboratory of Automobile Materials of MOE, Jilin University, Changchun 130012, China*

²*State Key Laboratory of Superhard Materials, Jilin University, Changchun 130012, China*

³*Department of Materials Science & Metallurgy, University of Cambridge, 27 Charles Babbage Road, Cambridge CB3 0FS, United Kingdom*

⁴*Theory of Condensed Matter Group, Cavendish Laboratory, J J Thomson Avenue, Cambridge CB3 0HE, United Kingdom*

⁵*Department of Physics and Astronomy, University of Missouri, Columbia, MO 65211-7010 USA*

(Dated: March 29, 2016)

The recent breakthrough discovery of unprecedentedly high temperature superconductivity of 203 K in compressed sulfur hydrides has stimulated significant interest in finding new hydrogen-containing superconductors and elucidating the physical and chemical principles that govern these materials and their superconductivity. Here we report the prediction of high temperature superconductivity in the family of pnictogen hydrides using first principles calculations in combination with global optimization structure searching methods. The hitherto unknown high-pressure phase diagrams of binary hydrides formed by the pnictogens of phosphorus, arsenic and antimony are explored, stable structures are identified and their electronic, vibrational and superconducting properties are investigated. We predict that SbH_4 and AsH_8 are high-temperature superconductors at megabar pressures, with critical temperatures in excess of 100 K. The highly symmetrical hexagonal SbH_4 phase is predicted to be stabilized above about 150 GPa, which is readily achievable in diamond anvil cell experiments. We find that all phosphorus hydrides are metastable with respect to decomposition into the elements within the pressure range studied. Trends based on our results and data in the literature reveal a connection between the high-pressure behaviors and ambient-pressure chemical quantities which provides insight into understanding which elements may form hydrogen-rich high-temperature superconducting phases at high pressures.

PACS numbers:

I. INTRODUCTION

Superconductivity, especially at high temperatures, continues to offer surprises both from experimental discoveries and theoretical insights often stimulated by these experiments. These findings include the Fe-based superconductors [1] which have provided a large body of theoretical work on spin-fluctuation pairing, nematicity and multiorbital physics [2–4], and recent reports of superconductivity in sulfur hydrides at pressures ~ 200 GPa with a T_c of 203 K [5, 6]. Superconducting sulfur hydrides show a strong isotope effect when deuterium is substituted for hydrogen, as expected for electron-phonon-based superconductivity [5]. This breakthrough observation has led to debate on the superconducting mechanism, including discussion of the limits of standard Migdal-Eliashberg electron-phonon coupling (EPC) theory [7–9], the role of strong covalent bonding [10, 11], the effects of anharmonicity on EPC [12], *etc.* These

proposals, together with the pioneering work of Ashcroft and coworkers on predicted high-temperature superconductivity in solid hydrogen [13] and in hydrogen-rich hydrides [14, 15] may guide research towards the discovery of new high-temperature superconductors based on materials containing light elements.

High-temperature superconductors can be divided into two classes: unconventional superconductors characterized by non-phonon primary pairing interactions, normally leading to non-standard pairing states, and conventional superconductors, with dominant electron-phonon pairing, and s-wave (or mainly s-wave for non-centrosymmetric cases) pairing states. In the latter case, methods exist for reliably evaluating superconducting properties and analyzing the superconductivity, *e.g.*, through calculating the Eliashberg EPC spectral function $\alpha^2F(\omega)$. A general consensus has been reached that the recently discovered superconducting sulfur hydrides belong to this category [5, 10, 16–19]. The experimental discovery was motivated by a theoretical prediction of high- T_c superconductivity in compressed solid H_2S by some of us [16]. Two superconducting states are observed in H_2S : samples prepared at low temperature have a maximum T_c of ~ 150 K at 200 GPa, while the superconductivity at 203 K arises from samples prepared via annealing at temperatures above 220 K. The latter phase originates

*These two authors contributed equally to this work.

†Electronic address: lijun.zhang@jlu.edu.cn

‡Electronic address: singhdj@missouri.edu

§Electronic address: mym@jlu.edu.cn

from the decomposition of H_2S into H_3S [6, 12, 17].

Theoretical predictions of high-temperature superconductivity rely on knowledge of the stable structures of the system. Global optimization structure searching methods [20] can identify previously unknown ground-state structures such as sulfur hydrides at high pressures [12, 16, 17, 21]. Calculations based on density functional theory (DFT) allow an accurate energetic evaluation of the structures found within the potential energy landscape and an assessment of their potential for superconductivity. The experimental discovery of high-temperature superconducting sulfur hydrides demonstrates the predictive power of DFT-based structure searching and EPC calculations, and suggests that more superconductors could be discovered using this approach. The role of theory is especially important since under such extreme conditions sample synthesis and *in situ* measurements of properties are usually challenging. Recently, the sister systems of selenium and tellurium hydrides were predicted to exhibit high- T_c superconductivity in hydrogen-rich compounds stabilized above 100 GPa [22, 23]. These proposals await experimental testing.

Here we explore the thermodynamic stability of pnictogen hydrides of P, As and Sb at high pressures and their superconducting properties. This investigation is in part motivated by the fact that the strength of the covalent H–P bond (with a bond energy of 322 kJ/mol) is rather similar to that of the H–S bond (bond energy of 363 kJ/mol) in the molecular gas phase. It is therefore reasonable to conjecture, within the scenario that strong covalent bonding favors superconductivity [10, 11], that phosphorus hydrides containing strong covalent bonds to H atoms and becoming metallic under compression might exhibit similarly strong EPC and potentially high- T_c superconductivity. To the best of our knowledge, solid pnictogen hydrides, even at ambient conditions, have only rarely been studied [24–27], although the corresponding molecular gases (*e.g.*, PH_3 , P_2H_4 , AsH_3 , and SbH_3) are well known in chemistry.

We find that thermodynamic stability of the gas molecules ($\text{PH}_3 > \text{AsH}_3 > \text{SbH}_3$) is reversed at high pressures, resulting in decomposition enthalpies that decrease from P, As to Sb hydrides. Except for the molecular solid phases stabilized by weak van der Waals interactions at low pressures [24–27], P hydrides are found to exhibit thermodynamic instability to decomposition into the elements under pressures up to 400 GPa. For As hydrides, stable compounds emerge only above 300 GPa. Sb hydrides are the most easily stabilized compounds above 150 GPa, which is readily achievable in diamond anvil cells. We have identified two stable hydrogen-rich compounds, SbH_4 and AsH_8 , as possible high-temperature superconductors with a T_c of 102 K at 150 GPa and 141 K at 350 GPa, respectively. Based on analysis of current and prior theoretical work on other binary hydrides, we have established a connection between ambient-pressure chemical properties and energetic sta-

bility, structural features, superconducting properties, *etc.* of hydrides upon pressures. The trends implied by this connection may help in discovering new binary and multinary high-pressure hydrogen-rich superconductors, since it does not require knowledge of the very different chemistries of elements at high pressures. Using trends in behavior to help in discovering superconductors has long been recognized, starting with the rules set out by Matthias [28, 29]. Finally, we mention the puzzling fact that although there have been more than a dozen predictions of high-temperature superconductivity in compressed hydrogen-rich compounds [16, 17, 19, 22, 23, 30–39], sulfur hydride is the only system to date that has been demonstrated to exhibit a higher superconducting temperature than the record of 164 K set by cuprates [40]. The second higher- T_c material identified in experiments is silicon hydride with $T_c = 17$ K around 100 GPa, [41], although the origin of the superconductivity is still under debate (likely from platinum hydride) [42, 43]. The chemical and physical properties of sulfur hydride that make it the highest- T_c superconductor found so far are not yet fully understood. Here we provide insight into this puzzle based on trends derived from data for a wide range of high-pressure hydrides.

II. COMPUTATIONAL APPROACHES

Our investigation consists of determination of stable stoichiometries and crystalline structures, and calculation of their superconducting and related properties. The hitherto unknown high-pressure phase diagrams (at 0 K) of pnictogen (X) hydrides were explored by performing very extensive structure searches for a set of stoichiometries X_nH_m , and the most stable structure and low-lying enthalpy metastable structures were identified for each X_nH_m . These calculations were performed using two leading codes for first-principles structure prediction, CALYPSO [44, 45] and AIRSS [46, 47]. The energetically stable stoichiometries and the most stable structure at each stoichiometry obtained from the two searching methods are in agreement. Over 100 stoichiometries were searched and a total of about 100,000 structures were relaxed by minimizing the total energy within the P/H, As/H and Sb/H systems.

DFT calculations were performed using the VASP code [48] with projected-augmented-wave (PAW) [49] potentials, and the CASTEP code with ultrasoft pseudopotentials. The $1s$ (H), $3s$ and $3p$ (P), $4s$ and $4p$ (As), and $5s$ and $5p$ (Sb) electrons were treated explicitly as valence electrons. We used the generalized gradient approximation exchange-correlation functional of Perdew, Burke and Ernzerhof [50]. Medium quality computational parameters were used when evaluating the enthalpies of structures during the searches. The low-lying enthalpy structures were then further optimized using the PAW method and more accurate computational parameters consisting of kinetic energy cutoff energies of 650 eV

(P/H and As/H) and 510 eV (Sb/H), and k-point meshes of spacing $2\pi \times 0.03 \text{ \AA}^{-1}$ or less. We checked the energy convergence with respect to these parameters and found convergence of the enthalpy differences to better than 1 meV/atom level.

We calculated the phonon dispersion relations and EPC using linear response theory as implemented in the Quantum ESPRESSO package [51]. These calculations were performed using norm-conserving pseudopotentials and a kinetic energy cutoff of 100 Ry. For reliable evaluation of the double-delta function integrals in the EPC calculations, dense k-point meshes with a spacing of about $2\pi \times 0.015 \text{ \AA}^{-1}$ were used, in combination with the Methfessel-Paxton broadening scheme [52] with a broadening parameter of 0.05 Ry. For the Brillouin sampling of phonon momentum, a q -point mesh with a grid spacing of $\sim 2\pi \times 0.06 \text{ \AA}^{-1}$ was adopted.

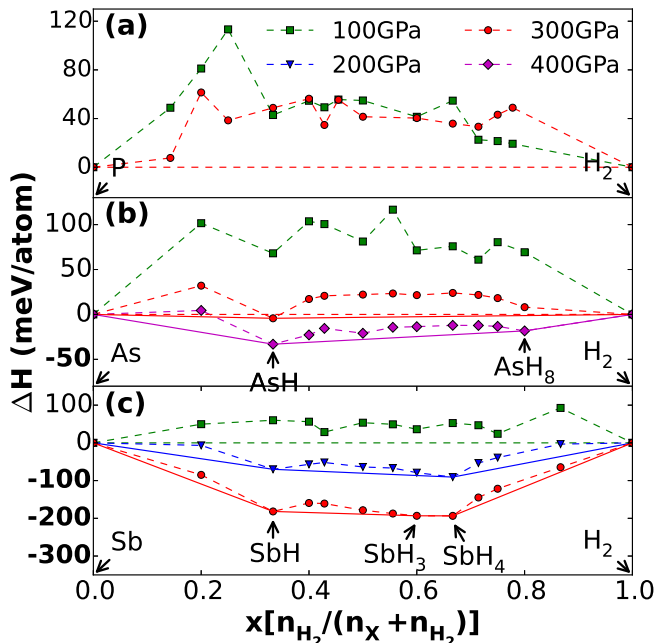


FIG. 1: (color online) Calculated formation enthalpies ΔH (in meV/atom) of various pnictogen hydrides with respect to decomposition into the elemental solids at 100 (squares), 200 (triangles), 300 (circles) and 400 (diamond) GPa, respectively. The data for each stoichiometry corresponds to the lowest enthalpy structures from the searches. The structures of phases VI ($Pm\bar{3}m$) and VIII ($Im\bar{3}m$) of P [53], IV ($Im\bar{3}m$) of As [53], III ($Im\bar{3}m$) of Sb [53], and the $P6_3m$ and $C2/c$ structures of solid H_2 [54] were used for evaluating ΔH .

III. RESULTS AND DISCUSSION

3.1 Phase stabilities and stable crystalline structures of pnictogen hydrides at high pressures. Since H-rich compounds are potentially more favorable for high-temperature superconductivity [14], we

focused our CALYPSO searches on the X_nH_m ($n=1\sim 3$ and $m=1\sim 8$) stoichiometries with higher H contents ($m \geq n$) containing up to 4 formula units per simulation cell. More diverse stoichiometries (with m up to 13) were considered in the AIRSS searches. The main results from these cross-checking search calculations are depicted in the hull diagrams of Fig. 1, which each contain data for pressures of 100–300 GPa. For As hydrides (Fig. 1b), searches at the higher pressure of 400 GPa were performed to demonstrate the stability of the AsH and AsH₈ structures above 300 GPa. Only the lowest enthalpy structure at each stoichiometry studied is shown.

We find a surprising trend in that at high pressures the thermodynamic stability of pnictogen hydrides increases with the atomic number of the pnictogen. The P hydrides (Fig. 1a) are found to be unstable against decomposition into the elements, and pressure does not have a noticeable effect on their stability. The predicted lowest-energy structures of several metastable stoichiometries are shown in Supplementary Fig. S1 and Table S1. As and Sb hydrides (Fig. 1b and 1c) show a clear tendency to be stabilized by increasing pressure; for As hydrides, a single stoichiometry stable against elemental decomposition into the elements emerges at 300 GPa, while for Sb hydrides, all the stoichiometries become stable above 200 GPa. These results indicate that the relative stabilities of the pnictogen hydrides obtained from the known chemical bonding strengths at ambient conditions ($P > As > Sb$) are opposite to those found at high pressures ($P < As < Sb$). We find two stable binary As hydrides on the convex hull at 400 GPa, AsH and AsH₈. We find three compounds on the convex hull for Sb hydrides at 300 GPa and two at 200 GPa. These are SbH, SbH₃ (at 300 GPa only) and SbH₄. Note that the much lower formation enthalpies of Sb hydrides (~ 200 meV/atom more stable) demonstrates their high stability under compression. We evaluated the effect of zero point energy (ZPE) on the phase stability by calculating harmonic phonon spectra for Sb hydrides, as shown in Supplementary Fig. S2. Inclusion of the ZPE gives rise to a negligible change in the convex hulls.

The structures of the predicted stable compounds are shown in Fig. 2a-e (see Supplementary Table S2 for detailed structural information), and the pressure ranges within which they are stable are depicted in Fig. 2f. The stable structures of the compounds remain unchanged throughout their stable pressure ranges. The AsH hydride (Fig. 2a) adopts a structure of $Cmcm$ symmetry which is stable above 300 GPa. It consists of a three-dimensional As-H network in which both As and H atoms are approximately five-fold coordinated. The lowest enthalpy structure of AsH₈ (Fig. 2b) of $C2/c$ symmetry is stabilized above 350 GPa. It is formed from the primary motifs of irregular AsH₁₆ polyhedra, connected with each other in a three-dimensional network. Each corner H atom of the AsH₁₆ polyhedron is linked to another H from the adjacent polyhedron. The short contact between two H atoms leads to formation of an intriguing

quasi-molecular H_2 -unit with a bond length of ~ 0.8 – 0.9 Å. The formation of such H_2 -units in compressed hydrides is also seen in systems with Si, Ge, Sn, Li, Ca, Te [23, 30, 32, 33, 55, 56], etc.

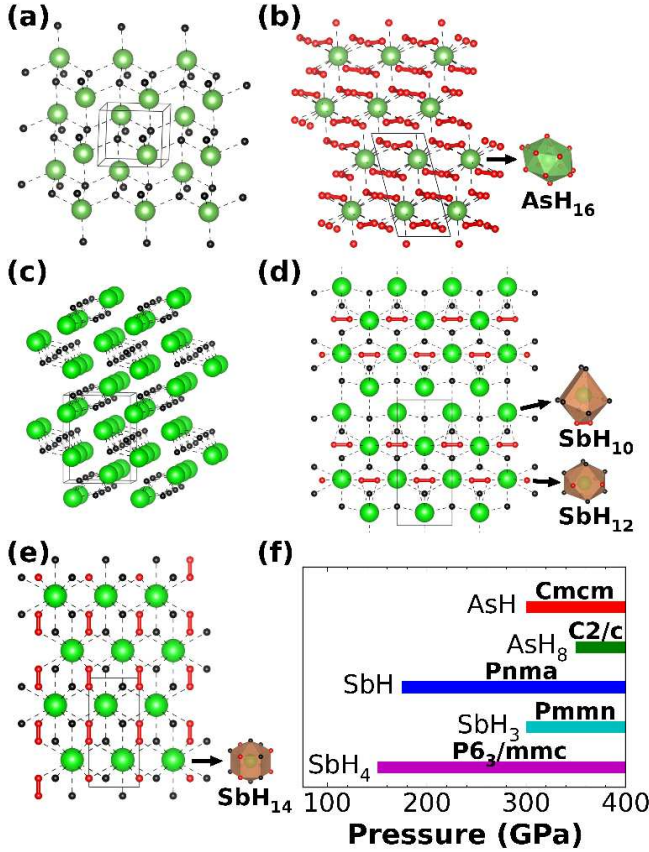


FIG. 2: (color online) Structures of the predicted stable pnictogen hydrides: (a) AsH (space group $Cmcm$), (b) AsH_8 ($C2/c$), (c) SbH ($Pnma$), (d) SbH_3 ($Pmmn$); (e) SbH_4 ($P6_3/mmc$). The As/Sb–H bonds are depicted by dashed lines and H–H covalent bonds as red sticks. The corresponding stable pressure range of each compound is shown in (f).

The energetically favored structure of SbH (Fig. 2c, stable above 175 GPa) has space group $Pnma$ and is composed of chain-like Sb–H motifs with each Sb coordinated by three H atoms. The H-rich compounds SbH_3 (Fig. 2d) and SbH_4 (Fig. 2e) have $Pmmn$ and $P6_3/mmc$ symmetries, respectively. While the former is marginally stable (very close to the convex hull formed by SbH and SbH_3 in Fig. 1c) at 300 GPa, the latter is robustly stable above 150 GPa. SbH_3 is composed of irregular polyhedral SbH_{10} and SbH_{12} motifs which form its three-dimensional topology. Bridging the adjacent SbH_{12} motifs in a two-dimensional fashion gives rise to quasi-molecular H_2 -units (in red) with a rather long bond length of ~ 0.91 Å, compared with the molecular H_2 bond length of 0.74 Å. SbH_4 is a highly symmetrical hexagonal compound that consists of SbH_{14} octadecahe-dra connected via shared H atoms at the corners to form

a three-dimensional network. There are two types of H atoms occupying the 4e (black) and 4f (red) Wyckoff sites, respectively. Each 4e H atom is coordinated by three Sb atoms, and the 4f H atom, while coordinated by two Sb atoms, has a close contact with another 4f H atom, forming quasi-molecular H_2 -units with a bond length of ~ 0.83 Å. SbH_4 resembles the TeH_4 compound with the same stoichiometry which adopts the $R\bar{3}m$ phase [23].

A Bader charge density analysis [57] shows substantial charge transfer from As/Sb to H (see Supplementary Table S3). This indicates that the As/Sb–H bonds have substantial ionic character. On the other hand, plots of the electron localization function (ELF) (see Supplementary Fig. S5) show material-dependent (see below) charge concentration between As/Sb and H atoms. Hence the predicted stable compounds are dominated by mixed covalent and ionic interactions.

3.2 Electronic structure, phonons, electron-phonon coupling and superconductivity of identified stable pnictogen hydrides. The DFT calculations indicate that all of the compounds are metallic within their stable pressure ranges. Fig. 3 shows band structures and projected densities of states (DOS) for three H-rich compounds, AsH_8 , SbH_3 and SbH_4 (see Supplementary Fig. S3 for results for H-poor AsH and SbH). The Fermi levels (E_f) of AsH_8 (Fig. 3a-b) and SbH_4 (Fig. 3e-f) are located at shoulders of a peak in the DOS, leading to a rather large value of the DOS at E_f ($N(E_f)$). Moreover, substantial H-derived states exist in proximity to E_f , which mimics solid metallic hydrogen. These features are potentially favorable for high-temperature superconductivity. This is, however, not the case for SbH_3 (Fig. 3c-d) in which E_f lies near the bottom of a broad valley in the DOS, which gives a low $N(E_f)$, and only a small amount of H derived states at E_f .

As shown in the phonon spectra of Fig. 4 (a: AsH_8 , d: SbH_3 and g: SbH_4) and Supplementary Fig. S4 (AsH and SbH), all of the compounds are dynamically stable as demonstrated by the absence of imaginary phonon frequencies. The projected phonon DOS of SbH_4 (Fig. 4h) shows three well separated regions: the low-frequency vibrations associated with heavy Sb atoms (below 15 THz), higher frequency wagging, bending and stretching modes derived from the H atom bonded to Sb (between 15 and 65 THz) and high-frequency intra-molecular H–H stretching modes from the quasi-molecular H_2 -units (around 80 THz). The H–H stretching modes of SbH_3 (Fig. 4e) are lower in frequency and they merge into the medium-frequency region because of the larger bond lengths of the H_2 -units. In AsH_8 (Fig. 4b), two groups of H–H stretching modes appear, which correspond to two types of H_2 unit with different bond lengths.

We performed EPC calculations for the predicted stable compounds to probe their superconducting properties. Fig. 4 shows the EPC parameters for each phonon mode (a,d,g), the Eliashberg EPC spectral function $\alpha^2F(\omega)$ and its integral $\lambda(\omega)$ (c,f,i) for AsH_8 , SbH_3 and

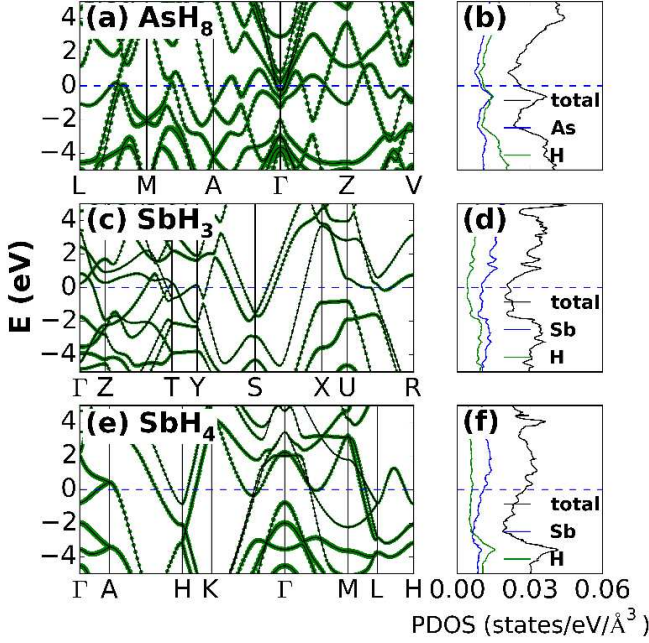


FIG. 3: (color online) Calculated band structures and projected densities of states of stable H-rich pnictogen hydrides: (a,b) AsH₈ at 350 GPa, (c,d) SbH₃ at 300 GPa and (e,f) SbH₄ at 150 GPa. The green circles in the band structures represent the orbital projections of the electronic states onto H atoms.

SbH₄ (results for AsH and SbH are shown in Supplementary Fig. S4). Fig. 5a summarizes data for the total EPC parameters λ and their pressure dependence. AsH₈ and SbH₄ are H-rich compounds with rather high λ values above 1.0, while SbH₃ has a lower value of about 0.5. For all three H-rich compounds the intermediate-frequency H-derived wagging, bending and stretching phonons and low-frequency vibrations from the heavy As/Sb atoms, rather than the high-frequency phonons derived from the H₂-units, dominate the contributions to the total EPC.

Within the framework of strong-coupling BCS theory [58], the total EPC parameter is proportional to the product of $N(E_f)$ and the squared electronic matrix element $\langle I^2 \rangle$ averaged over the Fermi surface. The calculated values of $N(E_f)$ for each compound are shown in Fig. 5b. While AsH₈ and SbH₄ have rather high values of $N(E_f)$, SbH₃ exhibits quite a low $N(E_f)$. These results accord with their significantly different λ values. The high $N(E_f)$ in H-poor AsH arises predominantly from As-induced states (Supplementary Fig. S3b) and results in a small value of λ similar to that of superconducting solid As under compression [59, 60]. Besides the difference in $N(E_f)$, we find that the strengths of the covalent components of As/Sb–H bonds (with mixed covalent and ionic nature) vary considerably among the compounds, as indicated by the ELF data shown in Supplementary Fig. S5. The Sb–H bonds in SbH₃ are much weaker than those of SbH₄ and the As–H bonds in AsH₈. The weaker Sb–H

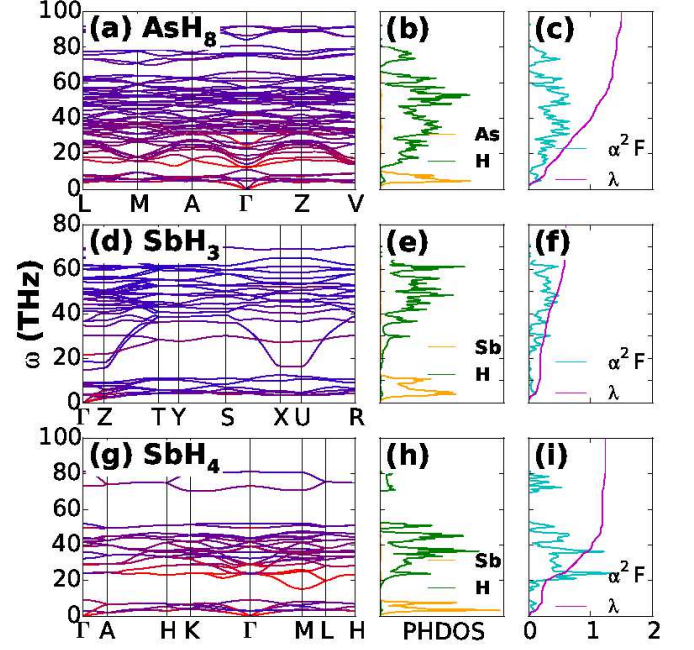


FIG. 4: (color online) Calculated phonon dispersion curves (a,d,g), projected phonon density of states (PHDOS) (b,e,h), Eliashberg EPC spectral functions $\alpha^2F(\omega)$ and its integral $\lambda(\omega)$ (c,f,i) of AsH₈ at 350 GPa, SbH₃ at 300 GPa and SbH₄ at 150 GPa, respectively. The proportion of red color in the phonon dispersion curves represents the magnitude of the EPC parameter $\lambda_{n,q}(\omega)$ at each phonon mode (n, q).

bonds in SbH₃ in principle correspond to a low deformation potential, *i.e.*, a smaller modification of the electronic structure, with respect to the motion of H atoms. This leads to a relatively small $\langle I^2 \rangle$, and thus a low λ .

The superconducting T_c values of the stable compounds are evaluated using the Allen-Dynes modified McMillan equation [61] with calculated logarithmic average frequency (ω_{log}) and a typical choice of screened Coulomb repulsion parameter of $\mu^* = 0.1$. The results shown in Fig. 5c (see Supplementary Table S4 for numerical values) are consistent with the trends in λ (Fig. 5a). AsH₈ and SbH₄ exhibit quite high T_c values of around 150 K and 100 K, respectively. The other compounds have moderate T_c values of ~ 20 K or below. The value of T_c in SbH₄ decreases slightly with pressure, while AsH₈ shows an increase. Using a standard value of $\mu^* = 0.13$ for metallic hydrides [14], we find a small decrease in T_c with pressure, ~ 8 –11% in the higher- T_c compounds of AsH₈ and SbH₄.

3.3 Deduced general chemical trends of high-pressure hydrogen-containing superconductors. Gathering data for pnictogen hydrides and other hydrides [12, 22, 23, 30–38, 62, 63] allows us to deduce useful physical principles about the phase stability and occurrence of high-temperature superconductivity in H-containing materials under pressure. For clarity, here we consider only the binary hydrides M_nH_m formed by main-group

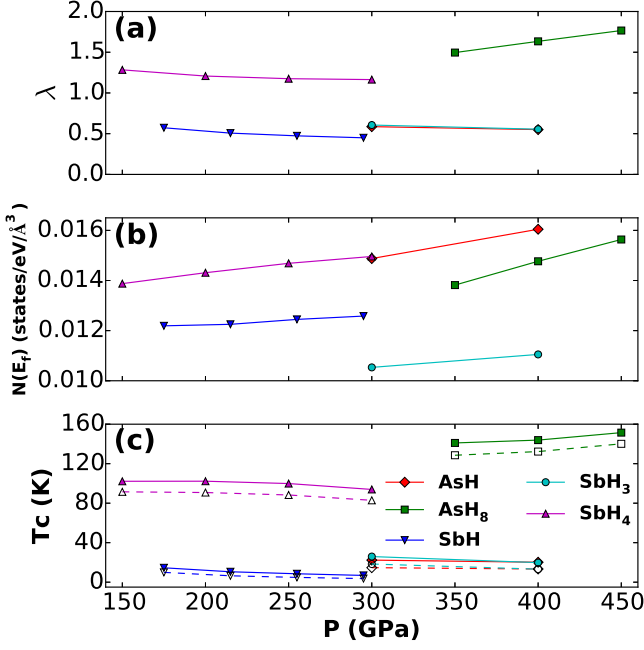


FIG. 5: (color online) The total EPC parameter λ (a), electronic DOS at the Fermi level $N(E_f)$ (b) and superconducting critical temperature T_c (c) as a function of pressure for the predicted stable compounds. For the T_c calculations, two different screened Coulomb repulsion parameters of $\mu^* = 0.1$ (filled symbols and solid lines) and 0.13 (open symbols and dashed lines) are used for comparison.

elements M with *sp* bonding. We find that the Pauling electronegativity difference between M and H at ambient pressure, $\chi_M - \chi_H$, is a good “descriptor” of high-pressure phase stability, structural features and superconducting properties of the hydrides. Specifically, we find that the following properties of M_nH_m are related to $\chi_M - \chi_H$:

(i) *Energetic stability against elemental decomposition.*

Fig. 6 shows formation enthalpies of various hydrides at 200 GPa as a function of $\chi_M - \chi_H$. For cases in which more than one stable stoichiometry exists, the averaged formation enthalpy (among all the stoichiometries) is shown, accompanied by an error bar indicating the maximum and minimum enthalpy. The diameter of the circular symbol is proportional to the atomic radius of M [64]. This divides hydrides into two classes with negative and positive $\chi_M - \chi_H$, respectively. Considering the extreme cases, H_2O with $\chi_M - \chi_H \gg 0$ has strong covalent O–H bonds, whereas LiH with $\chi_M - \chi_H \ll 0$ has strong ionic Li–H bonding. It may thus be reasonable to conjecture that the hydrides with $\chi_M - \chi_H > 0$ prefer to form covalent M–H bonds, while those with $\chi_M - \chi_H < 0$ are more ionic in nature. In the regions of both $\chi_M - \chi_H > 0$ and $\chi_M - \chi_H < 0$, we observe a general trend that the formation enthalpy decreases (*i.e.*, stability increases) with $|\chi_M - \chi_H|$. For $\chi_M - \chi_H > 0$, this can be explained by the larger electronegativity of M

which corresponds to strongly covalent M–H bonds, and therefore to higher stability of the hydrides. In this region, the atomic radius can also affect the covalent bond strength, and therefore have a critical role in determining the stability. For instance, despite the similar electronegativities of S and Se, S hydrides have much lower formation enthalpies than Se hydrides (by about 50~150 meV/atom). We attribute this to the smaller atomic radius of S favoring stronger covalent H–S bonds. In the region $\chi_M - \chi_H < 0$, the smaller electronegativity of M and larger value of $|\chi_M - \chi_H|$ leads to substantial charge transfer from the cationic M to anionic H. On the one hand, this increases the Madelung energy of the ionic component of the M–H bonding, which increases the stability. On the other hand, the charge transfer is favorable for the formation of quasi-molecular H units in the interstitial regions (see below). This lowers the enthalpy of hydrides and make them more stable. This explanation accords with the increased thermodynamic stability of P, As, and Sb hydrides, as demonstrated above.

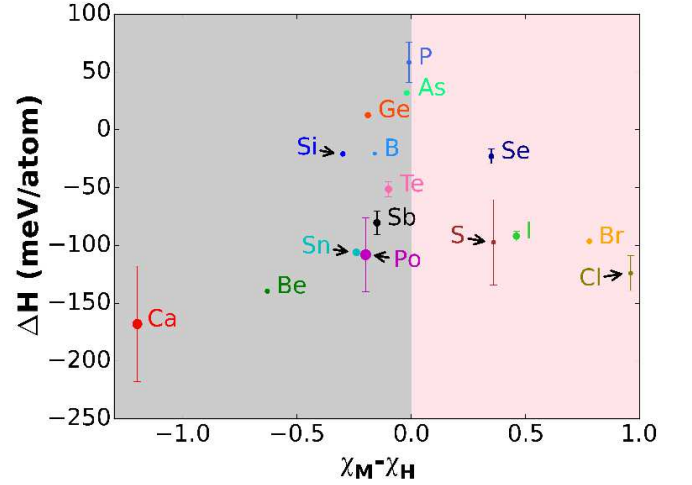


FIG. 6: (color online) Formation enthalpies ΔH (in meV/atom) of main-group-element (M) binary hydrides [12, 22, 23, 30–38, 62] at 200 GPa with respect to decomposition into the constituent elemental solids, plotted against the electronegativity difference between M and H at ambient pressure, $\chi_M - \chi_H$. The electronegativity values are taken from Pauling’s scale [65]. When several stable phases with different stoichiometries exist, the averaged formation enthalpy is shown, and the endpoints of the error bars represent the minimum and maximum values of ΔH . The sizes of the circles are proportional to the empirical atomic radii [64]. The regions corresponding to positive and negative $\chi_M - \chi_H$ are shown in the background colors of pink and gray, respectively.

(ii) *Key structural features.* For the hydrides with $\chi_M - \chi_H < 0$, for example our predicted AsH_8 , SbH_3 and SbH_4 phases, there is substantial charge transfer from the relatively electropositive M to the electronegative H (Supplementary Table S3). The M–H bonds have mixed covalent and ionic nature. With such weaker M–H bonding, the H atoms are prone to move to the in-

terstitial regions under pressures. Therefore, substantial energy gain may be achieved via the formation of H–H covalent bonds in the interstitial regions. This is especially the case under pressure where large non-bonded anions are unfavorable. This leads to the formation of intriguing quasi-molecular H-units in H-rich compounds [23, 30–33, 55, 66]. Turning to $\chi_M - \chi_H > 0$, for instance S [12, 16, 17] and Se [19, 22] hydrides, the strong polar covalent M–H bonds dominate. Under such conditions, all cationic H atoms are tightly bonded by the M atoms with large electronegativity, and thus the formation of H–H bonds is energetically unfavourable. The quasi-molecular H-unit is absent in the hydrides. The distinction between this key structural behavior in the two regions is reflected in Fig. 7, which shows the evolution of the CALYPSO search for SbH_4 ($\chi_M - \chi_H < 0$) and SeH_3 ($\chi_M - \chi_H > 0$) at 200 GPa. Usually tens of generations are required to determine the global minimum in the CALYPSO calculations. The structures at each generation are sorted according to their enthalpy. The color coding represents the minimum distance between two H atoms in each structure. All of the low enthalpy structures of SbH_4 contain quasi-molecular H_2 units with short contacts (0.8~0.9 Å) between neighboring H atoms. In contrast, in SeH_3 the low-lying structures exhibit large minimum H–H distances (over 1.5 Å) as three-dimensional covalent H–Se networks are formed.

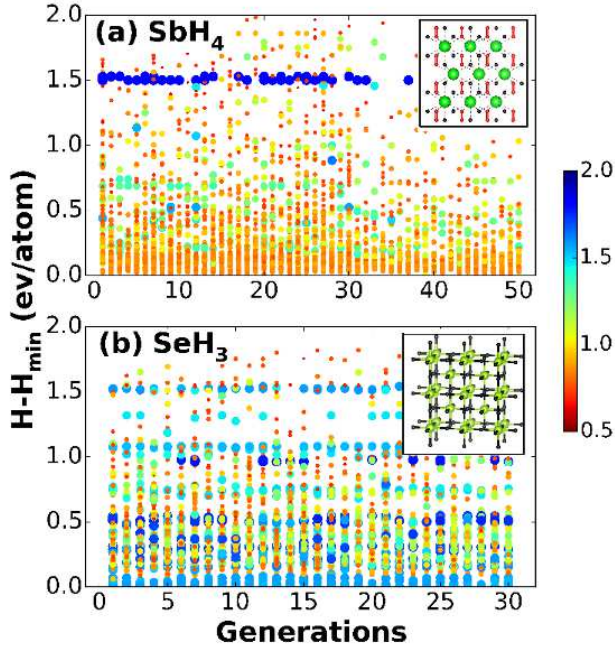


FIG. 7: (color online) The structures generated are sorted according to enthalpy during the CALYPSO structure searches for SbH_4 (a) and SeH_3 (b) at 200 GPa, as a function of search generations. The color-coding represents the minimum distance between two H atoms, which is also proportional to the size of the circle. The insets show the predicted ground-state structures of SbH_4 and SeH_3 .

(iii) *Density of states at the Fermi level.* As demonstrated in Fig. 5b, $N(E_f)$ is a critical parameter in determining the strength of the EPC. Fig. 8 shows the values of $N(E_f)$ for the binary hydrides that are predicted to be superconductors [12, 22, 23, 30–35, 37–39, 62, 63], as a function of $\chi_M - \chi_H$ at 200 GPa. To make a fair comparison and avoid potential errors arising from different theoretical calculations, we take structural data from Ref. 12, 22, 23, 30–35, 37–39, 62, 63, and perform full structural optimizations and calculate $N(E_f)$ using the plane-wave PAW method. In general, we find that high values of $N(E_f)$ appear in the region with relatively small magnitudes of $\chi_M - \chi_H$. The compounds with higher values of $N(E_f)$ in the two regions are TeH_4 , SbH_4 ($\chi_M - \chi_H < 0$) and SH_3 , SeH_3 ($\chi_M - \chi_H > 0$), respectively. The highly symmetric structures of these hydrides (TeH_4 : $P6/mmm$; SbH_4 : $P6_3/mmc$; S/ SeH_3 : $Im\bar{3}m$), which in principle give rise to high degeneracy of the band structure at special k -points, may be responsible for the high values of $N(E_f)$. They are all predicted to be good superconductors with values of λ above 1 [12, 17, 19, 22, 23].

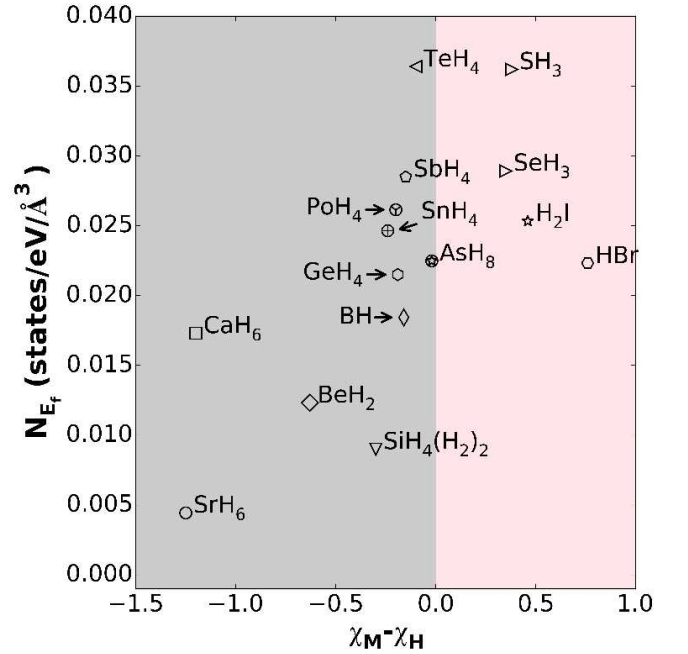


FIG. 8: (color online) Calculated electronic DOS at the Fermi level $N(E_f)$ of main-group-element binary hydrides [12, 22, 23, 30–35, 37–39, 62, 63] at 200 GPa, as a function of the electronegativity difference between M and H at ambient pressure, $\chi_M - \chi_H$. When several stable phases with different stoichiometries exist, we choose the one with the highest predicted superconducting T_c . Similar to Fig. 6, the regions of $\chi_M - \chi_H > 0$ and $\chi_M - \chi_H < 0$ are in pink and grey, respectively.

(iv) *Features of the electron-phonon coupling.* Fig. 9 shows the Eliashberg spectral function $\alpha^2F(\omega)$ (black lines), its normalized integral $\lambda(\omega)$ (divided by the to-

tal λ , colorful scale), and logarithmic average frequency ω_{log} (black scale) of typical compounds from the two regions. In the $\chi_M - \chi_H < 0$ region (AsH_8 and SbH_4), the total EPC originates mainly from the medium-frequency phonons, predominantly wagging, bending, and stretching modes derived from the H bonded to As/Sb. The higher frequency H-H stretching modes of the quasi-molecular H_2 -units make fairly small contributions to the EPC. Therefore the integral $\lambda(\omega)$ becomes saturated (in blue) at the upper-middle part of the ω range. Turning to the region of $\chi_M - \chi_H > 0$ (SH_3 and SeH_3), the EPC arises mainly from the high-frequency H-derived phonons of covalent M-H networks. The integral $\lambda(\omega)$ thus becomes saturated close to the upper boundary of ω . These features of the EPC can be ascribed to the different chemical bonding and structural features of the hydrides in the two regions. Note that ω_{log} , the important quantity determining the superconducting T_c , shows higher values in the $\chi_M - \chi_H > 0$ region than in the $\chi_M - \chi_H < 0$ region, despite the evidently lower maximum ω of the former region than that of the latter. This demonstrates that simply hardening the phonons is not always effective in raising T_c . The reason originates from the distinct dependence of $\alpha^2F(\omega)$ on ω in the two regions, since only the phonons contributing to the EPC are counted when evaluating T_c .

3.4 More relevant discussion. Since Ashcroft first proposed metallic hydrides as potentially good superconductors at high pressures [14], high- T_c (above 100 K) superconductivity has been predicted in a number of high-pressure H-rich compounds [12, 17, 22, 23, 30, 31]. The S hydride is one of these predictions [16, 17] that has been confirmed experimentally [5, 6]. In other systems, either low temperature superconductivity [41, 67] or no superconductivity [68, 69] was found. While the underlying reasons for this are not yet settled, one possibility is that the predicted superconducting compounds did not form in high-pressure experiments. Confining hydrides or mixtures of hydrogen and other substances in diamond anvil cells up to ultrahigh pressure conditions is technically challenging and, due to the technical limitations, experimental syntheses may fail even though the theoretically predicted structures are energetically stable. This is highly likely for hydrides with small formation enthalpies, such as those of Si, Ge, B, Se, *etc.*, as indicated in Fig. 6.

It is also possible that kinetic processes under pressure inhibit formation of some of the predicted compounds. If so, a highly symmetric structure may be more likely to be synthesised because the energetic barrier for the transition between the symmetric structure and other isomers is usually large. This suggests a strong kinetic stability with respect to variations in the external conditions. From this point of view, S hydrides are indeed favorable for experimental synthesis since the stable SH_3 structure has simultaneously a large formation enthalpy (~ 135 meV/atom at 200 GPa) and high symmetry (space group $Im\bar{3}m$). In this sense, the SbH_4 phase predicted in the

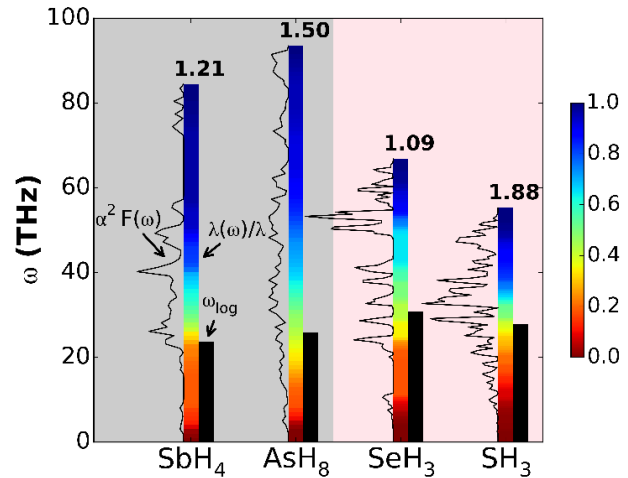


FIG. 9: (color online) The Eliashberg EPC spectral function $\alpha^2F(\omega)$ (black lines), its integral $\lambda(\omega)$ (colorful scale), and logarithmic average frequency ω_{log} (black scale) for typical hydrides in the regions of $\chi_M - \chi_H > 0$ (SH_3 and SeH_3) and $\chi_M - \chi_H < 0$ (AsH_8 and SbH_4). For comparison among different compounds, the $\lambda(\omega)$ is normalized and divided by the total λ (indicated for each compound).

present work is quite promising for possible experimental synthesis, in view of its large formation enthalpy (~ 90 meV/atom at 200 GPa) and highly symmetric structure (space group $P6_3/mmc$). Certainly the larger barrier associated with the highly symmetric structure may make its synthesis challenging. This can be basically overcome by for instance sufficient thermal energy or catalytic assistant.

Turning to trends, results from the current and previous theoretical studies reveal a connection between the thermodynamic stability, structural features and superconducting properties of high-pressure hydrides, and the Pauling electronegativity differences between H and the other elements. This is a remarkable and at first sight strange finding, since high-pressure chemistry is well known to be radically different from that at ambient pressure [70]. Our findings indicate that the ambient-pressure chemical properties determine to a large extent the high-pressure behavior.

Electropositive elements (with $\chi_M - \chi_H \ll 0$ in our classification), such as alkaline and alkaline earth metals, form highly ionic ambient-pressure hydrides characterized by large charge transfers and structures similar to fluorides. In particular, the crystals are stabilized by the Madelung energy of the cationic M and anionic H ions. The anionic H in these materials are well separated from other H ions and the H vibrational frequencies are relatively low. At high pressures the distances between H anions are significantly shortened, but the weak ionic M-H bonds allow H atoms to move to the interstitial regions. These lead to stabilization of the H-H covalent bonds in the interstitial region. Thus quasi-molecular aggregation

of H emerges [30, 55, 63, 66] and high H vibrational frequencies occur in the high-pressure phases.

Non-metallic strongly electronegative elements (with $\chi_M - \chi_H \gg 0$) often form weakly bound insulating H-containing molecular solids at ambient pressure, *e.g.*, NH_3 , H_2O , H_2S , *etc.* While strong covalent M–H bonds dominate molecules, the intermolecular bonds characterizing cohesion of molecular solids are weak van der Waals bonds and hydrogen bonds. Under compression, with decreasing intermolecular distances and accompanying hydrogen-bond symmetrization [71–73], solids with covalent M–H bonding networks eventually become energetically favored. Because of the strong polar covalent M–H bonds, the H–H bonds and aggregation of H atoms are energetically unfavourable.

As for the elements with moderate electronegativities comparable to that of H ($\chi_M - \chi_H \sim 0$), the hydrides formed are intermediate between the above two cases. The M–H bonds have mixed covalent and ionic characters, and the former is not strong enough to stabilize covalently bonded M–H networks. In the hydrides with $\chi_M - \chi_H < 0$ (Si, Ge, Sn, Te, Sb, *etc.*), the anionic nature of H atoms (due to the charge transfer from M to H) and the tendency of H atoms to move to interstitial regions (due to the relatively weak M–H bonds) under pressure allows aggregation of H via formation of H–H covalent bonds in H-rich phases. This mechanism helps to stabilize hydrides. The stability increases with the magnitude of $\chi_M - \chi_H$ (as in Fig. 6), which determines the Madelung energy of the ionic interaction and the capability of hydrides to form aggregates of H. For As and P hydrides with small $|\chi_M - \chi_H|$, only limited charge transfer from As/P to H can occur due to the small electronegativity difference. On the other hand, the fairly strong As/P–H covalent bonds hinder H atoms from moving to interstitial regions. Hence H–H covalent bonds are unlikely to form. This may be responsible for their positive formation enthalpies in Fig. 6.

Once metallic hydrides are stabilized by high pressure, one can ask whether or not they are good superconductors. Our current results indicate that three features of hydrides are essential for strong EPC and a high T_c . The first is a high $N(E_f)$. While this quantity certainly depends on the specific band structure and electronic occupation, highly symmetric structures are in principle favorable for high values of $N(E_f)$. Interestingly this occurs with small magnitudes of $|\chi_M - \chi_H|$ (Fig. 8). The second feature is the appearance of substantial H-derived states in proximity to E_f , mimicking pure metallic hydrogen. H-rich compounds are more likely to satisfy this criterion. The third feature is the large electronic deformation potential with respect to motion of H atoms. The hydrides with strong chemical bonding, especially covalent bonding, are more favored by this feature. In this regard, the T_c of S hydrides are predicted to be enhanced by alloying with more electronegative elements (*e.g.*, P and O) [11, 74] to further strengthen the covalent bonding. For the hydrides containing quasi-molecular assemblies of H

atoms [23, 30–34, 55, 63, 66, 75], the deformation potential associated with intra-molecular H–H stretching motion is fairly large (due to the strong H–H covalent bonds). Unfortunately, as demonstrated in Fig. 9, the corresponding phonon modes make a quite limited contribution to the EPC. An even higher superconducting T_c would be expected if these phonon modes were involved in the EPC, for example, under further compression.

While preparing this manuscript, our attention was drawn to two reports on superconductivity in pnictogen hydrides. One is a preliminary observation of high T_c superconductivity in P hydrides from ~ 30 K increasing continuously to more than 100 K up to pressures above 200 GPa [76]. While more experimental data are required to verify this finding, the basic idea coincides with the main motivation of this work. However, based on our structure searching results, P hydrides are predicted to be unstable against elemental decomposition up to 400 GPa. Our results point to the possibility that P hydrides formed in the experiments [76] may be metastable and could be stabilized by kinetic processes at high pressures. The conclusion that the P hydrides are thermodynamically unstable at megabar pressures is consistent with recent theoretical reports [77, 78]. Further analysis of the metastability, energy barriers related to kinetic stability, as well as superconductivity calculations for P hydrides, will be published elsewhere. Another is the theoretical prediction of 106 K superconductivity in SbH_4 at 150 GPa by Ma *et al.* [79]. Using a structure searching method based on a genetic algorithm [80], they obtained the same high-symmetry structure (space group $P6_3/mmc$) of SbH_4 that we have found in our work. Their calculations of superconducting properties also agree with ours. Experimental attempts to synthesise Sb hydrides at high pressures and explore their superconducting properties are eagerly anticipated to test this theoretical prediction.

IV. IV. CONCLUSIONS

We have used first principles structure searching methods to study the hitherto unknown phase diagram of solid pnictogens (*i.e.*, P, As, Sb) hydrides at high pressures with the aim of predicting new high- T_c superconductors. Surprisingly, except for the molecular solid phases stabilized by weak van der Waals interactions near ambient pressure, we did not find any P hydrides to be stable with respect to decomposition into the elements up to 400 GPa. The hydrides containing the heavy element Sb are found to be the most stable at high pressures. This was unexpected because at ambient pressure the lighter pnictogen hydrides are the most stable.

We have predicted several stable superconducting hydrides (AsH , AsH_8 , SbH , SbH_3 and SbH_4). Among them, two H-rich compounds, AsH_8 and SbH_4 are predicted to exhibit T_c values of ~ 150 K above 350 GPa, and ~ 100 K above 150 GPa, respectively. SbH_4 is energetically very

stable and adopts a highly symmetrical hexagonal structure, and the stabilization pressure is well within reach of modern diamond anvil cell experiments. Finally, through systematic analysis of current and previous studies of binary hydrides, we determined a close connection between the high-pressure behavior of hydrides and ambient pressure chemical quantities. In particular we found that the electronegativity difference between the constituent elements is a good descriptor for characterizing the structure, chemical bonding, thermodynamic stability and superconducting properties of hydrides at high pressures. Analysing these trends could provide further insights into the intriguing and diverse chemical and physical properties of compressed hydrides. Our work provides a useful roadmap for discovering more stable compressed hydrides and exploration of their superconducting properties.

ASSOCIATED CONTENT

Supporting Information. Effect of zero point energy on phase stabilities, Electronic structure, phonon, electron-phonon coupling results of H-poor compounds, Electron localization function and Bader charge analy-

sis results, Explicit structural information and calculated superconducting properties of the identified stable hydrides.

ACKNOWLEDGMENTS

The authors thank Eva Zurek for sharing structure data for iodine hydride. The work at Jilin Univ. is supported by the funding of National Natural Science Foundation of China under Grant Nos. 11274136 and 11534003, 2012 Changjiang Scholar of Ministry of Education and the Postdoctoral Science Foundation of China under grant 2013M541283. L.Z. acknowledges funding support from the Recruitment Program of Global Youth Experts in China. Part of calculations was performed in the high performance computing center of Jilin Univ. R.J.N. acknowledges financial support from the Engineering and Physical Sciences Research Council (EPSRC) of the UK [EP/J017639/1]. R.J.N. and C.J.P. acknowledge use of the Archer facility of the U.K.'s national high-performance computing service (for which access was obtained via the UKCP consortium [EP/K013564/1]).

-
- [1] Y. Kamihara, T. Watanabe, M. Hirano, and H. Hosono, *J. Am. Chem. Soc.* **130**, 3296 (2008).
 - [2] C. Fang, H. Yao, W.-F. Tsai, J. Hu, and S. A. Kivelson, *Phys. Rev. B* **77**, 224509 (2008).
 - [3] I. I. Mazin, D. J. Singh, M. D. Johannes, and M. H. Du, *Phys. Rev. Lett.* **101**, 057003 (2008).
 - [4] D. J. Scalapino, *Rev. Mod. Phys.* **84**, 1383 (2012).
 - [5] A. P. Drozdov, M. I. Erements, I. A. Troyan, V. Ksenofontov, and S. I. Shylin, *Nature* **525**, 73 (2015).
 - [6] M. Einaga, M. Sakata, T. Ishikawa, K. Shimizu, M. Erements, A. Drozdov, I. Troyan, N. Hirao, and Y. Ohishi, p. arXiv:1509.03156 (2015).
 - [7] E. J. Nicol and J. P. Carbotte, *Phys. Rev. B* **91**, 220507 (2015).
 - [8] A. Bianconi and T. Jarlborg, p. arXiv:1507.01093 (2015).
 - [9] J. Hirsch and F. Marsiglio, *Phys. C* **511**, 45 (2015).
 - [10] N. Bernstein, C. S. Hellberg, M. D. Johannes, I. I. Mazin, and M. J. Mehl, *Phys. Rev. B* **91**, 060511 (2015).
 - [11] C. Heil and L. Boeri, *Phys. Rev. B* **92**, 060508 (2015).
 - [12] I. Errea, M. Calandra, C. J. Pickard, J. Nelson, R. J. Needs, Y. Li, H. Liu, Y. Zhang, Y. Ma, and F. Mauri, *Phys. Rev. Lett.* **114**, 157004 (2015).
 - [13] N. W. Ashcroft, *Phys. Rev. Lett.* **21**, 1748 (1968).
 - [14] N. W. Ashcroft, *Phys. Rev. Lett.* **92**, 187002 (2004).
 - [15] J. Feng, W. Grochala, T. Jaroń, R. Hoffmann, A. Bergara, and N. W. Ashcroft, *Phys. Rev. Lett.* **96**, 017006 (2006).
 - [16] Y. Li, J. Hao, H. Liu, Y. Li, and Y. Ma, *J. Chem. Phys.* **140**, 174712 (2014).
 - [17] D. Duan, Y. Liu, F. Tian, D. Li, X. Huang, Z. Zhao, H. Yu, B. Liu, W. Tian, and T. Cui, *Sci. Rep.* **4**, 6968 (2014).
 - [18] D. A. Papaconstantopoulos, B. M. Klein, M. J. Mehl, and W. E. Pickett, *Phys. Rev. B* **91**, 184511 (2015).
 - [19] J. A. Flores-Livas, A. Sanna, and E. K. U. Gross, p. arXiv:1501.06336 (2015).
 - [20] Y. Wang and Y. Ma, *J. Chem. Phys.* **140**, 040901 (2014).
 - [21] D. Duan, X. Huang, F. Tian, D. Li, H. Yu, Y. Liu, Y. Ma, B. Liu, and T. Cui, *Phys. Rev. B* **91**, 180502 (2015).
 - [22] S. Zhang, Y. Wang, J. Zhang, H. Liu, X. Zhong, H.-F. Song, G. Yang, L. Zhang, and Y. Ma, p. arXiv:1502.02607 (2015).
 - [23] X. Zhong, H. Wang, J. Zhang, H. Liu, S. Zhang, H.-F. Song, G. Yang, L. Zhang, and Y. Ma, p. arXiv:1503.00396 (2015).
 - [24] G. Natta and E. Casazza, *Gazz. Chim. Ital.* **60**, 981 (1930).
 - [25] P. Sennikov, *J. Phys. Chem.* **98**, 4973 (1994).
 - [26] M. Baudler and K. Glinka, *Chem. Rev.* **93**, 1623 (1993).
 - [27] A. Holleman and E. Wiberg, *Inorganic Chemistry* (Academic Press, München, 2001).
 - [28] B. Matthias, *Progress in low temperature physics*, vol. 2 (North Holland Publishing Company, Leiden, 1957).
 - [29] D. Pines, *Phys. Rev.* **109**, 280 (1958).
 - [30] H. Wang, J. S. Tse, K. Tanaka, T. Iitaka, and Y. Ma, *Proc. Natl. Acad. Sci. U.S.A.* **109**, 6463 (2012).
 - [31] Y. Li, G. Gao, Y. Xie, Y. Ma, T. Cui, and G. Zou, *Proc. Natl. Acad. Sci. U.S.A.* **107**, 15708 (2010).
 - [32] G. Gao, A. R. Oganov, A. Bergara, M. Martinez-Canales, T. Cui, T. Iitaka, Y. Ma, and G. Zou, *Phys. Rev. Lett.* **101**, 107002 (2008).
 - [33] G. Gao, A. R. Oganov, P. Li, Z. Li, H. Wang, T. Cui, Y. Ma, A. Bergara, A. O. Lyakhov, T. Iitaka, et al., *Proc. Natl. Acad. Sci. U.S.A.* **107**, 1317 (2010).
 - [34] Y. Liu, D. Duan, F. Tian, D. Li, X. Sha, Z. Zhao, H. Zhang, G. Wu, H. Yu, B. Liu, et al., p.

- arXiv:1503.08587 (2015).
- [35] A. Shamp and E. Zurek, p. arXiv:1507.02616 (2015).
 - [36] D. Duan, F. Tian, X. Huang, D. Li, H. Yu, Y. Liu, Y. Ma, B. Liu, and T. Cui, p. arXiv:1504.01196 (2015).
 - [37] Z. Wang, Y. Yao, L. Zhu, H. Liu, T. Iitaka, H. Wang, and Y. Ma, *J. Chem. Phys.* **140**, 124707 (2014).
 - [38] C.-H. Hu, A. R. Oganov, Q. Zhu, G.-R. Qian, G. Frapper, A. O. Lyakhov, and H.-Y. Zhou, *Phys. Rev. Lett.* **110**, 165504 (2013).
 - [39] S. Lu, M. Wu, H. Liu, J. S. Tse, and B. Yang, *RSC Adv.* **5**, 45812 (2015).
 - [40] L. Gao, Y. Y. Xue, F. Chen, Q. Xiong, R. L. Meng, D. Ramirez, C. W. Chu, J. H. Eggert, and H. K. Mao, *Phys. Rev. B* **50**, 4260 (1994).
 - [41] M. I. Eremets, I. A. Trojan, S. A. Medvedev, J. S. Tse, and Y. Yao, *Science* **319**, 1506 (2008).
 - [42] O. Degtyareva, J. E. Proctor, C. L. Guillaume, E. Gregoryanz, and M. Hanfland, *Solid State Commun.* **149**, 1583 (2009).
 - [43] D. Szczesniak and T. P. Zemina, *Supercond. Sci. Technol.* **28**, 085018 (2015).
 - [44] Y. Wang, J. Lv, L. Zhu, and Y. Ma, *Phys. Rev. B* **82**, 094116 (2010).
 - [45] Y. Wang, J. Lv, L. Zhu, and Y. Ma, *Comput. Phys. Commun.* **183**, 2063 (2012).
 - [46] C. J. Pickard and R. J. Needs, *Phys. Rev. Lett.* **97**, 045504 (2006).
 - [47] C. J. Pickard and R. J. Needs, *J. Phys. Condens. Matter* **23**, 053201 (2011).
 - [48] G. Kresse and J. Furthmüller, *Phys. Rev. B* **54**, 11169 (1996).
 - [49] P. E. Blöchl, *Phys. Rev. B* **50**, 17953 (1994).
 - [50] J. P. Perdew, J. A. Chevary, S. H. Vosko, K. A. Jackson, M. R. Pederson, D. J. Singh, and C. Fiolhais, *Phys. Rev. B* **46**, 6671 (1992).
 - [51] P. Giannozzi, S. Baroni, N. Bonini, M. Calandra, R. Car, C. Cavazzoni, D. Ceresoli, G. L. Chiarotti, M. Cococcioni, I. Dabo, et al., *J. Phys. Condens. Matter* **21**, 395502 (2009).
 - [52] M. Methfessel and A. T. Paxton, *Phys. Rev. B* **40**, 3616 (1989).
 - [53] H. Katzke and P. Tolédano, *Phys. Rev. B* **77**, 024109 (2008).
 - [54] C. J. Pickard and R. J. Needs, *Nat. Phys.* **3**, 473 (2007).
 - [55] E. Zurek, R. Hoffmann, N. W. Ashcroft, A. R. Oganov, and A. O. Lyakhov, *Proc. Natl. Acad. Sci. U.S.A.* **106**, 17640 (2009).
 - [56] J. S. Tse, Y. Yao, and K. Tanaka, *Phys. Rev. Lett.* **98**, 117004 (2007).
 - [57] W. Tang, E. Sanville, and G. Henkelman, *J. Phys. Condens. Matter* **21**, 084204 (2009).
 - [58] W. L. McMillan, *Phys. Rev.* **167**, 331 (1968).
 - [59] A. L. Chen, S. P. Lewis, Z. Su, P. Y. Yu, and M. L. Cohen, *Phys. Rev. B* **46**, 5523 (1992).
 - [60] I. V. Berman and N. B. Brandt, *J. Exp. Theor. Phys. Lett.* **10**, 55 (1969).
 - [61] P. B. Allen and R. C. Dynes, *Phys. Rev. B* **12**, 905 (1975).
 - [62] Z. Wang, H. Wang, J. S. Tse, T. Iitaka, and Y. Ma, *Chem. Sci.* **6**, 522 (2015).
 - [63] Y. Wang, H. Wang, J. S. Tse, T. Iitaka, and Y. Ma, *Phys. Chem. Chem. Phys.* **17**, 19379 (2015).
 - [64] J. C. Slater, *J. Chem. Phys.* **41**, 3199 (1964).
 - [65] D. R. Lide, *CRC handbook of chemistry and physics* (CRC press, Boca Raton, 2004).
 - [66] P. Baettig and E. Zurek, *Phys. Rev. Lett.* **106**, 237002 (2011).
 - [67] T. Muramatsu, W. K. Wanene, M. Somayazulu, E. Vinit-sky, D. Chandra, T. A. Strobel, V. V. Struzhkin, and R. J. Hemley, *J. Phys. Chem. C* **119**, 18007 (2015).
 - [68] I. Goncharenko, M. I. Eremets, M. Hanfland, J. S. Tse, M. Amboage, Y. Yao, and I. A. Trojan, *Phys. Rev. Lett.* **100**, 045504 (2008).
 - [69] M. I. Eremets, V. V. Struzhkin, H. K. Wang Mao, and R. J. Hemley, *Physica B* **329**, 1312 (2003).
 - [70] R. Van Eldik and F.-G. Klärner, *High pressure chemistry* (John Wiley & Sons, Erlangen, 2008).
 - [71] C. Lee, D. Vanderbilt, K. Laasonen, R. Car, and M. Parrinello, *Phys. Rev. Lett.* **69**, 462 (1992).
 - [72] K. Aoki, H. Yamawaki, M. Sakashita, and H. Fujihisa, *Phys. Rev. B* **54**, 15673 (1996).
 - [73] K. R. Hirsch and W. B. Holzapfel, *J. Chem. Phys.* **84**, 2771 (1986).
 - [74] Y. Ge, F. Zhang, and Y. Yao, p. arXiv:1507.08525 (2015).
 - [75] V. V. Struzhkin, D. Kim, E. Stavrou, T. Muramatsu, H. Mao, C. J. Pickard, R. J. Needs, V. B. Prakapenka, and A. F. Goncharov, p. arXiv:1412.1542 (2014).
 - [76] A. P. Drozdov, M. I. Eremets, and I. A. Trojan, p. arXiv:1508.06224 (2015).
 - [77] A. Shamp, T. Terpstra, T. Bi, Z. Falls, P. Avery, and E. Zurek, ArXiv e-prints p. arXiv:1509.05455 (2015).
 - [78] J. A. Flores-Livas, M. Amsler, C. Heil, A. Sanna, L. Boeri, G. Profeta, C. Wolverton, S. Goedecker, and E. K. U. Gross, p. arXiv:1512.02132 (2015).
 - [79] Y. Ma, D. Duan, D. Li, Y. Liu, F. Tian, X. Huang, Z. Zhao, H. Yu, B. Liu, and T. Cui, p. arXiv:1506.03889 (2015).
 - [80] A. R. Oganov and C. W. Glass, *J. Chem. Phys.* **124**, 244704 (2006).

Supplemental Material for “High-pressure Phase Stability and Superconductivity of Pnictogen Hydrides and Chemical Trends for Compressed Hydrides”

Yuhao Fu,¹ Xiangbo Du,² Lijun Zhang,¹ Feng Peng,² Miao Zhang,² Chris J. Pickard,³ Richard J. Needs,⁴ David J. Singh,^{1,5} Weitao Zheng,¹ and Yanming Ma²

¹*College of Materials Science and Engineering and Key Laboratory of Automobile Materials of MOE, Jilin University, Changchun 130012, China*

²*State Key Laboratory of Superhard Materials, Jilin University, Changchun 130012, China*

³*Department of Materials Science & Metallurgy, University of Cambridge, 27 Charles Babbage Road, Cambridge CB3 0FS, United Kingdom*

⁴*Theory of Condensed Matter Group, Cavendish Laboratory, J J Thomson Avenue, Cambridge CB3 0HE, United Kingdom*

⁵*Department of Physics and Astronomy, University of Missouri, Columbia, MO 65211-7010 USA*
(Dated: March 29, 2016)

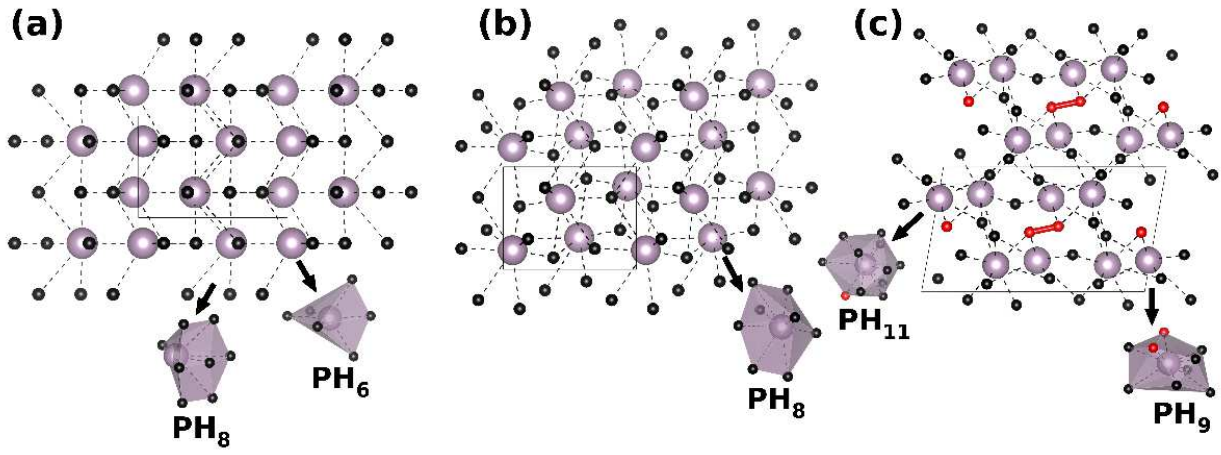


FIG. S1: (color online) Crystal structures of several predicted metastable P hydrides: (a) P_2H_3 (space group $P2_1/m$), (b) PH_2 space group $P2_1/c$, (c) PH_3 space group $C2/m$).

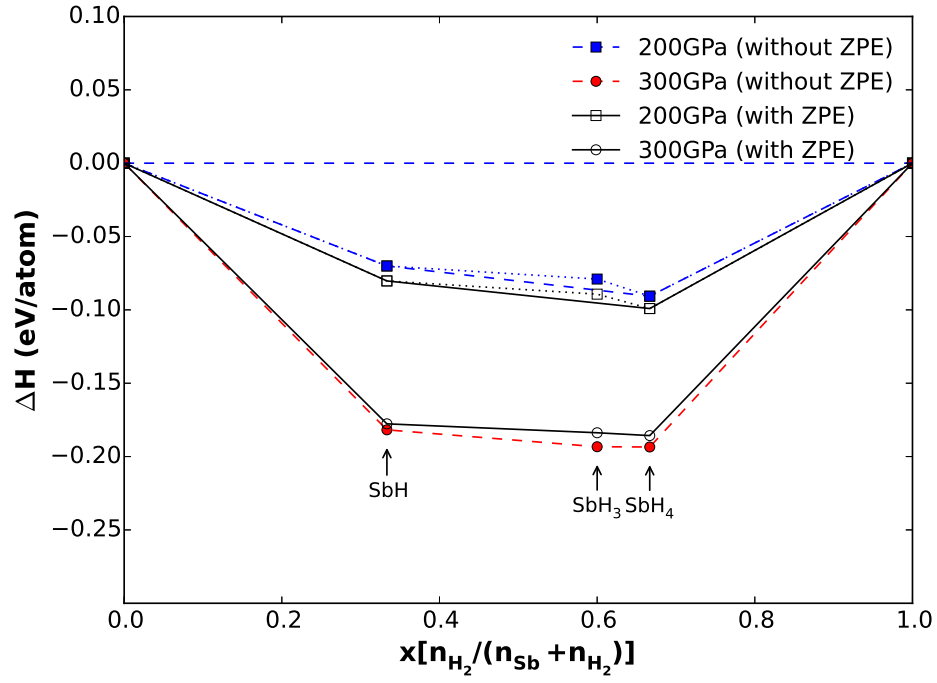


FIG. S2: (color online) Calculated formation enthalpy ΔH (in meV/atom) of predicted stable Sb hydrides at 200 and 300 GPa with (open symbols) and without (filled symbols) inclusion of zero point energy (ZPE) effects, respectively.

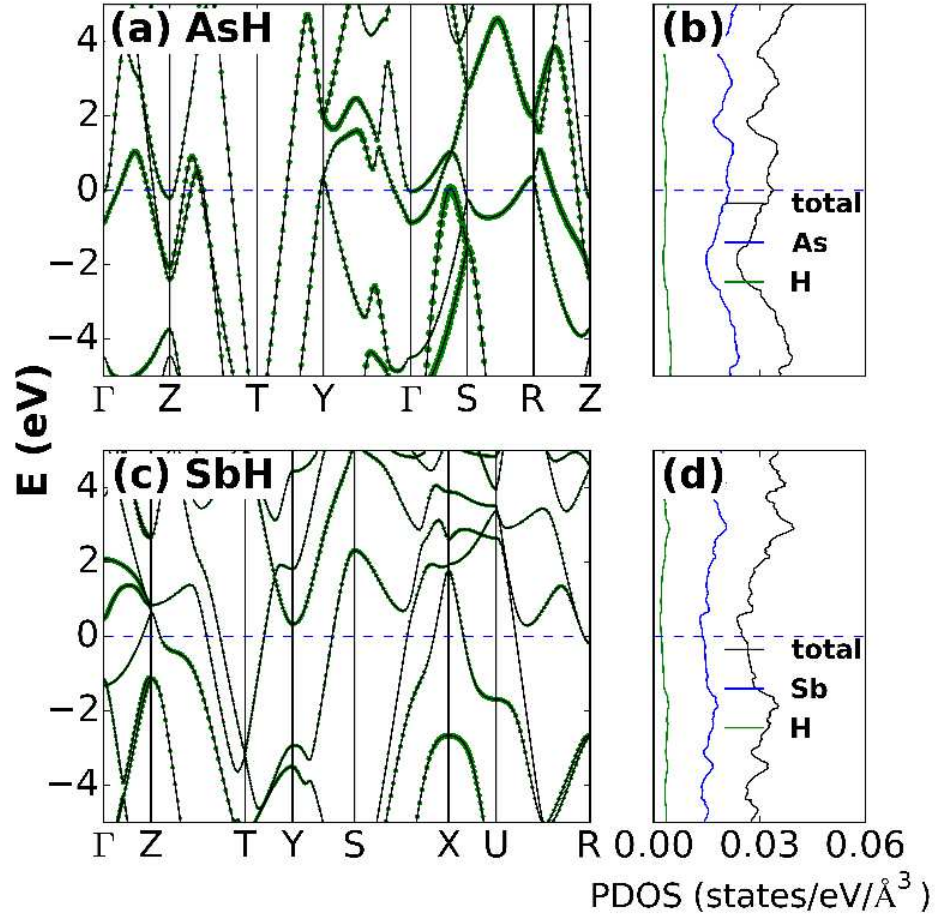


FIG. S3: (color online) Electronic band structure and projected density of states of (a,b) AsH at 350 GPa and (c,d) SbH at 300 GPa. The green circles in the band structures represent the orbital projection of the electronic states onto H atoms.

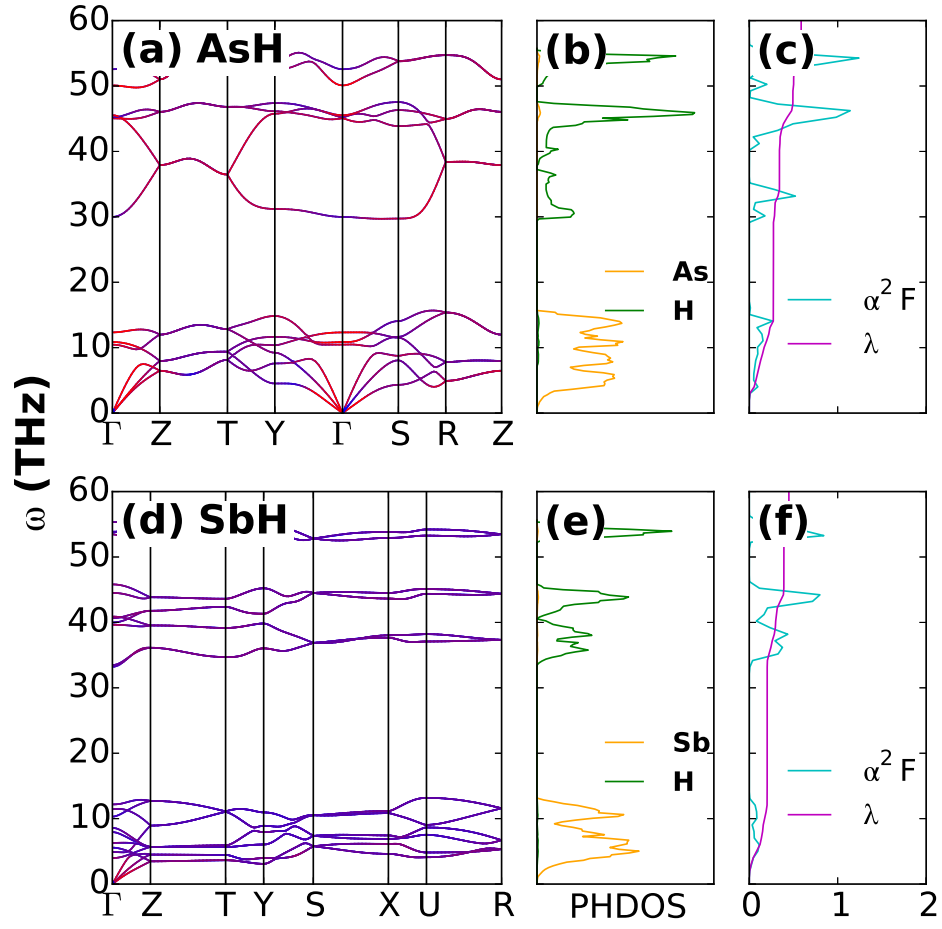


FIG. S4: (color online) Phonon dispersion curves (a,d), projected phonon densities of states (PHDOS) (b,e), Eliashberg EPC spectral functions $\alpha^2 F(\omega)$ and its integral $\lambda(\omega)$ (c,f) of AsH at 350 GPa and SbH at 300 GPa. The proportion of red color in the phonon dispersion curves represents the magnitude of the EPC parameter $\lambda_{n,q}(\omega)$ at each phonon mode (n, q) .

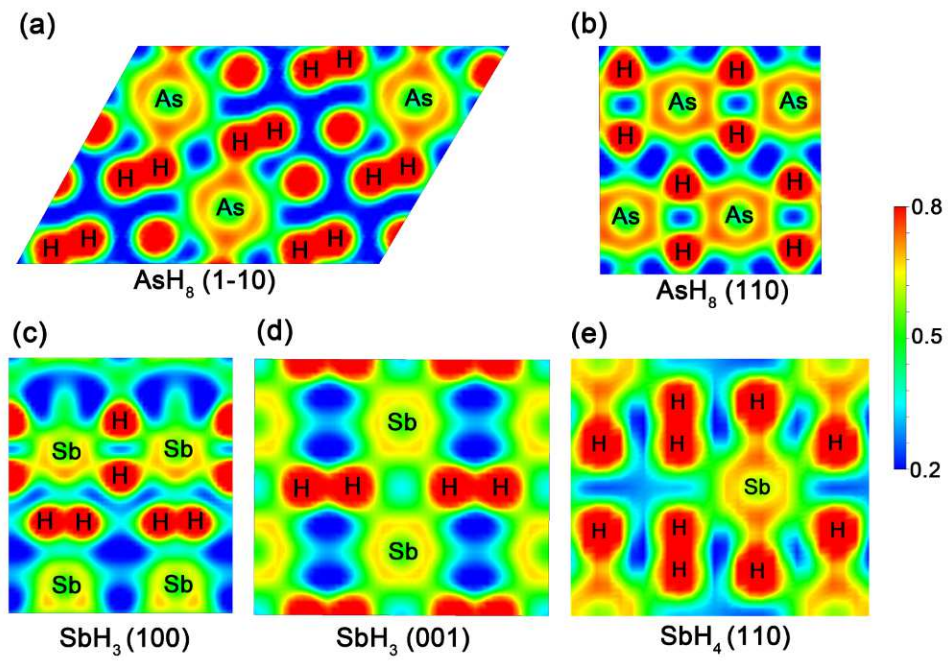


FIG. S5: (color online) Two-dimensional contour plots of the electron localization function for AsH_8 (a,b), SbH_3 (c,d) and SbH_4 (e), respectively. The planes containing As/Sb-H bonds are chosen to show the bonding character.

TABLE S1: Detailed structural information of several predicted metastable P hydrides.

Phase (pressure)	Lattice parameters (\AA , $^\circ$)	Atomic coordinates (fractional)			
$\text{P}_2\text{H}_3 - P2_1/m$ (300GPa)	a=4.142	P (2e)	0.970	0.250	0.239
	b=2.825	P (2e)	0.377	0.250	0.657
	c=3.093	H (2e)	0.831	0.250	0.736
	$\alpha=\gamma=90$	H (2e)	0.386	0.750	0.002
	$\beta=89.838$	H (2e)	0.670	0.750	0.826
$\text{PH}_2 - P2_1/c$ (300GPa)	a=3.290	P (4e)	0.806	0.430	0.688
	b=3.920	H (4e)	0.253	0.187	0.297
	c=3.138	H (4e)	0.477	0.876	0.384
	$\alpha=\gamma=90$				
	$\beta=106.456$				
$\text{PH}_3 - C2/m$ (300GPa)	a=7.206	P (4i)	0.993	0.000	0.748
	b=3.093	P (4i)	0.813	0.500	0.785
	c=4.088	H (8j)	0.852	0.296	0.296
	$\alpha=\gamma=90$	H (4i)	0.213	0.000	0.064
	$\beta=100.029$	H (4i)	0.783	0.000	0.554
		H (4i)	0.936	0.500	0.106
		H (4i)	0.062	0.500	0.477

TABLE S2: Detailed structural information on the predicted stable pnictogen hydrides.

Phase (pressure)	Lattice parameters (\AA , $^\circ$)	Atomic coordinates (fractional)			
AsH- <i>Cmcm</i> (350GPa)	a=3.241	As (4c)	0.500	0.695	0.250
	b=4.156	H (4c)	0.500	0.932	0.750
	c=2.998				
	$\alpha=\beta=\gamma=90$				
AsH ₈ - <i>C2/c</i> (350GPa)	a=5.604	As (4e)	0.000	0.246	0.750
	b=2.813	H (8f)	0.263	0.397	0.394
	c=5.685	H (8f)	0.771	0.387	0.871
	$\alpha=\gamma=90$	H (8f)	0.131	0.253	0.072
	$\beta=120.033$	H (8f)	0.993	0.753	0.603
SbH- <i>Pnma</i> (300GPa)	a=2.771	Sb (4c)	0.356	0.750	0.212
	b=3.197	H (4c)	0.925	0.750	0.855
	c=3.9852				
	$\alpha=\beta=\gamma=90$				
SbH ₃ - <i>Pmmn</i> (300GPa)	a=2.771	Sb (2b)	0.000	0.500	0.101
	b=3.197	Sb (2b)	0.000	0.500	0.631
	c=7.284	H (4f)	0.738	0.000	0.150
	$\alpha=\beta=\gamma=90$	H (4e)	0.500	0.143	0.642
		H (2a)	0.000	0.000	0.535
		H (2a)	0.000	0.000	0.748
SbH ₄ - <i>P6₃/mmc</i> (300GPa)	a=2.783	Sb (2c)	0.667	0.333	0.750
	b=2.783	H (4e)	0.000	0.000	0.580
	c=5.217	H (4f)	0.333	0.667	0.581
	$\alpha=\beta=90$				
	$\gamma=120$				

TABLE S3: Bader charge analysis for the predicted stable pnictogen hydrides. Note that H represents monoatomic H atoms bonding with As/Sb, and H1, H2, H3 and H4 are the H atoms forming quasi-molecular H₂-units.

		population charge	
AsH- <i>Cmcm</i>	As	4.6885	0.3115
	H	1.3115	-0.3115
AsH ₈	As	4.1217	0.8783
	H1	1.1524	-0.1524
	H2	1.1248	-0.1248
	H3	1.0866	-0.0866
	H4	1.0753	-0.0753
SbH- <i>Pnma</i>	Sb	4.4666	0.5334
	H	1.5334	-0.5334
SbH ₃ - <i>Pmmn</i>	Sb1	3.9782	1.0218
	Sb2	3.5377	1.4623
	H1	1.3310	-0.3310
	H	1.4354	-0.4354
	H	1.4729	-0.4749
SbH ₄ - <i>P6₃/mmc</i>	Sb	3.5117	1.4883
	H1	1.2713	-0.2713
	H	0.1430	-0.4730

TABLE S4: Calculated total EPC parameter λ , logarithmic average frequency ω_{log} , electronic DOS at the Fermi level $N(E_f)$ and superconducting critical temperature T_c for the predicted stable pnictogen hydrides. The screened Coulomb repulsion parameter $\mu^* = 0.1$ is used for the T_c calculations.

Phase	Pressure (GPa)	λ	ω_{log} (K)	$N(E_f)$	T_c (K)
AsH- <i>Cmcm</i>	300	0.59	995	4.43	21.2
	400	0.55	1166	4.24	20.2
AsH ₈ - <i>C2/c</i>	350	1.50	1240	7.29	141.0
	400	1.63	1169	7.44	143.9
	450	1.77	1153	7.56	151.4
SbH- <i>Pnma</i>	175	0.57	736	10.40	14.6
	215	0.51	820	9.89	10.5
	255	0.47	877	9.59	8.5
	295	0.45	890	9.30	6.8
SbH ₃ - <i>Pmmn</i>	300	0.61	1100	9.25	25.9
	400	0.56	1112	8.89	19.8
SbH ₄ - <i>P6₃/mmc</i>	150	1.28	1054	8.07	102.2
	200	1.21	1133	7.68	102.3
	250	1.18	1145	7.38	99.9
	300	1.16	1090	7.12	93.9